3D implicit modeling applied to the evaluation of CO_2 geological storage in the shales of the Irati Formation, Paraná Basin, Southeastern Brazil

Saulo B. de Oliveira (sauloboliveira@hotmail.com)
Universidade de São Paulo Instituto de Energia e Meio Ambiente https://orcid.org/0000-0002-2149-1297

Colombo C. G. Tassinari
Universidade de Sao Paulo Instituto de Energia e Ambiente

Richardson M. A-A.
Universidade de Sao Paulo Instituto de Energia e Ambiente

Ignacio Torresi
Seequent Limited

Research Article

Keywords: CO2 geological storage, 3D geological modeling, carbon capture and storage, Irati Formation, Paraná Basin

Posted Date: July 21st, 2021

DOI: https://doi.org/10.21203/rs.3.rs-420789/v2

Version of Record: A version of this preprint was published at Greenhouse Gases: Science and Technology on August 11th, 2021. See the published version at https://doi.org/10.1002/ghg.2111.

Abstract

The Paris Agreement established global ambitious targets for reducing carbon dioxide (CO_2) emissions, requiring the rapid and extensive development of low carbon technologies, and one of the most efficient is CO_2 geological storage. Among the deep geological formations used for CO_2 storage, the shale layers have been a new emerging topic showing to be efficient because they are abundant and have a high content of organic matter, being favorable for CO_2 retention. However, one of the challenges in evaluating a location for possible reservoirs is the adequate geological characterization and storage volume estimates. This research evaluated the Irati Formation of the Paraná Basin, through the information from hydrocarbon exploration wells in Southeastern Brazil, where most stationary sources of carbon emissions are located. Three-dimensional (3D) implicit modeling techniques were applied not only for the volume calculation purpose, but also in the site selection stage, generating thematic 3D models of thickness, depth, structures, and distance to aquifer systems. The limestones, shales, and black shales of the Irati Formation were locally divided into six units according to geological composition and spatial continuity. The E black shale unit was considered for CO_2 geological storage indicating a theoretical capacity of 1.85 Gt of CO_2. The potential of the achieved capacity is promising not only for been greater than the total of CO_2 locally produced but also for supporting the implantation of new projects in this region.

Introduction

In a scenario of growth in the generation and emission of CO_2, the global emissions reached a historical record of about 33.1 billion tons (Gt) of CO_2 in 2018 according to the International Energy Agency.[1] Brazil is among the 20 countries with the highest CO_2 emissions in recent years.[1] The data provided by the *Sistema de Estimativas de Emissões e Remoções de Gases de Efeito Estufa (SEEG)* on CO_2 emissions by the Brazilian energy sector, based on the methodology of Azevedo *et al*,[2] indicates a significant increase from 173 million tons (Mt) of CO_2 in 1990 to 380 Mt of CO_2 in 2018.[3] Brazil has also set goals to contribute to the reduction of greenhouse gas emissions, aiming at 37% by 2025, and 43% by 2030, based on 2005 emissions, as stated in its Nationally Determined Contribution (NDC) ratification. This worldwide decision requires the rapid and extensive development of low carbon technologies, and one of the most efficient approaches is Carbon Capture and Storage (CCS). In the Brazilian context, CCS technologies are becoming relevant due to the CO_2 emission capacity of the energy sector, considering the development of technologies that respond positively to global trends.

Deep geological formations provide suitable repositories for CO_2 storage, however, some requirements must be met to allow large amounts of CO_2 to be injected and that the gas remains trapped in the rock for a long time.[4, 5] Usually depleted oil and gas fields, saline aquifers, deep salt formations (salt caves and abandoned mines), coal seams, basalt, and black shale layers are considered viable CO_2 reservoirs.[6, 7] Each of these types of CO_2 geological reservoirs has distinct trapping mechanisms, including structural/stratigraphic trapping, residual trapping, dissolution trapping, and mineral trapping.[8-10] The

efficiency of shale layers for CO_2 storage has gained popularity because they are abundant and have a high content of organic matter and clay minerals, which are favorable materials for CO_2 retention by adsorption. Besides, the shale layers may contain unconventional hydrocarbons (shale gas and shale oil). If shale oil and gas production becomes viable within the Irati Formation, the co-development of hydrocarbon wells and CO_2 storage will reduce cost.[11] Shale gas is an extensive global energy resource, and its development can integrate the CO_2 geological storage as a feasible technological alternative to reduce carbon emissions impact on the climate.[12, 13]

The research focuses on generating a three-dimensional (3D) geological model based on a pre-selected area measuring about 185,000 km² (Fig. 1) with potential for CO_2 storage in the São Paulo State, southeastern Brazil. The implicit geological modeling in a three-dimensional (3D) virtual environment[14-17] has been widely used in the mineral industry for at least 15 years. Recent examples of 3D implicit geological modeling include iron deposits (e.g. Sishen Mine, South Africa),[18] base metal deposits (e.g. Falunin Sweden, Flin Flon in Canada, and Shalipayco in Peru),[19-21] gold deposits (e.g. Navachab in Namibia, La Colossa in Colombia, and Sigma-Lamaque in Canada),[22-24] and geothermal reservoirs,[25] amongst others. The 3D implicit modeling expands the analysis of conventional geological data by visualizing continuities, groupings, and spatial trends, as well as geometries of geological bodies or units, structural geological framework, and variation of geochemical contents or any other numerical or categorical parameters in geosciences. Examples of 3D geological modeling focusing on CO_2 storage are scarce.[26-34] Evaluations and studies focusing on CO_2 geological storage in the Paraná Basin include the study based on the Santa Terezinha coalfield,[35] and those considering saline aquifers.[36-40] The objectives in this research include: 1) Site selection on a regional scale for CO_2 storage focusing on the shale reservoirs within the Paraná Basin, and 2) Estimation of the theoretical storage capacity of the selected site. The 3D geological model of Paraná Basin will aid the assessment of the geological feasibility of implementing CCS technology in Southeastern Brazil to reduce CO_2 in this region where most of the country's carbon emission stationary sources are concentrated.[37, 39, 41] Therefore, the innovations of this work are the first application of 3D implicit modeling to evaluate the CO_2 storage potential of the shale reservoirs in the study location, comprising the initial steps of Site Selection and Initial Characterization.[42] The study considered the hypothesis that the Irati Formation organic-rich shales present reservoir units with enough capacity to permanently store the volume of the waste CO_2 released to the atmosphere considering the emitting sources within the region.

Main Text

The dataset provided by ANP in December 2019 is composed of hydrocarbon exploration well data. The dataset contains data of collar, survey, lithology, stratigraphy, and hydrocarbon occurrence, as well as, wireline logs consisting of gamma-ray, resistivity, density, neutrons, and sonic log, besides some organic geochemistry data acquired by Petrobras Company during the 1950s until the 2000s. A filter was applied in a total of 123 wells in the Paraná Basin resulting in 32 wells in the study area (Fig. 1). From these

wells, all have stratigraphy data, 29 of the wells have some lithology data, and 15 have some hydrocarbon indication data. In Fig. 1 and subsequent figures, in the location indicated by the 3-CB-3-SP well label, there are also located other four wells (2-CB-1-SP, 2-CB-1DA-SP, 3-CB-2-SP, and 3-CB-4-SP) lying 3 km from each other on average. Therefore, their labels were omitted in the figures for a scale issue, to avoid overlaps and visual pollution. Almost all filtered wells are vertical with only one having survey data. Then, all available data were loaded in the Leapfrog Geothermal® software for performing three-dimensional (3D) geological modeling. The Leapfrog software uses radial basis functions (RBFs) to perform surfaces by the implicit modeling method.[14] It involves the generation of a regional surface topographic model based on the GTOPO30 data (https://earthexplorer.usgs.gov/). Surface geology data (lithology and structures) were obtained from Companhia de Pesquisa de Recursos Minerais (CPRM),[43] and regional geological structures are from Zalán,[44] and then treated in the free software QGIS Desktop before importing into Leapfrog platform.

THE IRATI FORMATION IN THE STUDY AREA

The Irati Formation occurs in almost the entire extension of the Paraná Basin.[45-47] In the study area, outcrops of the Irati Formation are restricted to the southeast portion only (Fig. 2). For this research, the classification of the lithologic units depends mainly on well logs data. Almost all the wells in the area penetrate the Irati Formation horizon, except for the 1-QT-1-PR well, which is very shallow, and the 1-TI-1-SP well, which presents an extensive diabase dike at intervals between the Teresina and Palermo Formations (Fig. 3). In the study area, 8 wells (1-J-1-PR, 1-MA-1-SP, 1-PA-1-SP, 1-SA-1-SP, 2-AA-1-SP, 2-AP-1-PR, 2-RI-1-PR, 2-TB-1-SP) present some punctual oil indication, 5 wells present gas indication (2-CB-1-SP, 2-CB-1DA-SP, 3-CB-2-SP, 3-CB-3-SP, 3-CB-4-SP), referring to the Cuiabá Paulista sub-commercial gas accumulation, and 4 wells show bitumen (1-AB-1-SP, 1-GU-4-SP, 2-PN-1-SP, and 2-PP-1-SP), all within the Irati Formation (Fig. 2).

A 3D interpretation of the lithology data with some TOC data enabled a subdivision of the Irati Formation into units following the subdivision of literature.[48-50] Due to the erratic availability of samples with TOC analysis, the three A, B, and C base units were undifferentiated and referred to as a single shale unit named Unit A/B/C (Fig. 3). This work considers six units informally named Units A/B/C to H from the bottom to the top (Fig. 3), to conform to the existing divisions.[48-50] The lithologic unit interpretation incorporates the thickness of units less than 1 m into the larger adjacent units. Therefore, larger shaly units may contain thin and discontinuous levels of limestone, and delineated carbonate units may also have incorporated thin-bedded shale levels. Unit A/B/C is a shale layer with incorporated carbonate layers having a thickness measuring up to 30 m at the middle of the study location and about 3 m at the eastern portion. The sequence from Units D to G is laterally continuous and occurs in the entire E-W section (Fig. 3) for more than 300 km across the study area. Unit D consists of limestones with incorporated dolostones, calcilutite to calcarenite having a thickness range of 1 to 16 m. The thickness of the organic-rich shale Unit E varies from 2 to 20 m. Both Units E and F consist of interbedded diabase sill in the eastern portion. Unit F is composed of shales with a thickness range of 1 to 14 m throughout the E-

W section. Unit G is composed of limestones and dolostones with grain size varying from calcilutite to calcarenite, and thickness in the wells ranges from 2 to 11 m. The topmost Unit H is an organic-rich shale layer that occurs only at the west of the study location. The presented Irati Formation subdivisions are similar to those showcased in Figure 4 and presented in the literature,[48-50] although it is not exactly equivalent.

INITIAL CRITERIA FOR SELECTING THE CO_2 STORAGE LOCATION

CO_2 stationary sources and some legal aspects

The study area (Fig. 1) already accounted for some of the CO_2 site selection criteria considering the region with the highest CO_2 stationary emitting sources and legal aspects. The land use, land-use change, and forestry (LULUCF) sector is the major net emitter of CO_2 in Brazil, followed by the energy sector. The São Paulo State is the state with the highest CO_2 emissions in the energy sector considering the concentration of thermoelectric power plants (Fig. 1).[37, 39, 51] Based on 2018 data, from the 380 Mt of CO_2 emitted in the Brazilian energy sector, 80 Mt (21%) is from the São Paulo State.[3] The Paraná State also has a high concentration of thermoelectric plants. However, the Paraná State Law 19.878 of 2019 prohibits the production of unconventional natural gas production through hydraulic fracking,[52] although the state has no oil and gas production activities. The Barra Bonita conventional gas field within the region is not producing. The legal context of shale gas in the Paraná Basin is better and deeply discussed in the literature.[52, 53] Brazil has no federal or states legal restrictions or specific legislation to prevent CCS.[54, 55] Therefore, areas inside the São Paulo State were prioritized in this study, mainly because of the high concentration of energy sector and biomass industries related to sugar-cane ethanol plants.[56]

Regional geological aspects

The Paraná Basin is tectonically related to a more than 10,000 km-long divergent margin originated by the Gondwana paleocontinent break-up and the separation of the African and South American plates,[57] with no relation with fold belts, therefore, it is a tectonically favorable location for CO_2 storage considering IEA-GHG recommendations.[58] The Paraná Basin in the southeast of Brazil presents a low level of seismic activity because it is a typical intra-plate region. Only five earthquakes with m_b magnitude above 5.0 (with two being of large-magnitude: 6.3 and 6.8) have occurred in the studied region for the past 220 years according to Berrocal,[59] and the bulletins of Centro de Sismologia da Universidade de São Paulo (USP), Brazil (http://moho.iag.usp.br/eq/bulletin). This scenario also indicates a favorable location for CO_2 reservoir based on IEA-GHG recommendations.[58]

Depth, thickness and distance to groundwater aquifers

To evaluate the subsurface depth, thickness, and distance to groundwater aquifers [58], 3D thematic models were built in the Leapfrog platform using lithology data from wells. These models were generated

using the *Vein type* software tool. For the depth of the Irati Formation (Fig. 5), all intervals immediately above the formation were selected, and then the model was generated. The thickness model (Fig. 6) was generated considering only the Irati Formation vertical intervals of the selected wells. For a model of the distance of the CO_2 reservoir until the aquifer systems in the area: Bauru, Serra Geral, and Guarani,[60] it was considered the deepest of them: the Guarani Aquifer,[61, 62] using the lithology intervals from the top of Irati Formation to the Botucatu and Piramboia Formations base (Fig. 7).

The depth of the Irati Formation increases in the west towards the depocenters of the basin exceeding 2,800 m (Fig. 5). The Irati Formation thickness varies from 22 to 64 m within the captured area (Fig. 6). In nine wells the Irati Formation thickness has shown outlier values from 94 to 265 m. The respective Irati Formation intervals in the database include some diabase intervals. To eliminate these outliers, the data were filtered to consider only the portions above the diabase. The distance between the top of the Irati Formation and the base of the Guarani Aquifer increases from the west exceeding 1,400 m outside the state of São Paulo in the east of the Mato Grosso do Sul state (Fig. 7).

3D IMPLICIT GEOLOGICAL AND STRUCTURAL MODELING

Regional-scale 3D geological and structural model

The 3D geological implicit modeling was built initially on a regional scale using the already interpreted stratigraphy data consisting of gamma-ray log with outlined geological formations and groups representing the study location (Fig. 2). 12 geological units were considered in the stratigraphic model from base to top: Paraná Group, Itararé Group, Rio Bonito Formation, Palermo Formation, Irati Formation, Serra Alta Formation, Teresina Formation, Rio do Rasto Formation, Piramboia Formation, Botucatu Formation, Serra Geral Formation, and Bauru Group. The study grouped the Corumbataí Formation data with Teresina Formation data. Descriptions of these units are according to literature.[46, 63] The contacts from the CPRM geological map were involved together with the wireline logs data from the eastern region of the study area where the geological formations are exposed.[43] It includes wells intervals selection and interpretation of the contact surfaces between each geological formation using the *Deposit type* software tool. Detailed descriptions of the cited software tools are available on the Seequent website (https://help.leapfrog3d.com/Geothermal/). The lithological model was based on wireline log data alone, with no use of trends or other software artifices to avoid bias or subjective interpretation. This approach aided to identify possible abrupt changes in the stratigraphic sequence that could indicate fault displacements.

The structural model was generated from the surface fault traces,[43, 44] which have been transformed into fault surfaces assuming a vertical dip for all. This simplified assumption is based on a characteristic of an extensional regime consisting of dominant steeply deep normal faults,[64] following the evolution of the Paraná Basin.[57, 63] The initial analysis for the site selection looked through regions with a low incidence of fractures or faults to avoid possible CO_2 leakages. The approach involves delineating geological formation contacts and activating the fault system in the software to generate fault-assisted blocks. It

also involves an empirical approach to active some faults and analyzes the displacement of blocks case by case considering the number of faults and lineaments. The goal was to locate possible structural traps for CO_2 storage. The final configuration of the structural model aided to generate seven fault assisted blocks (Fig. 8), considering six faults: 1) The Guaxupé Fault with an approximate N60E direction; 2) The Mogi Lineament with an E-W direction; 3) The São Jerônimo Fault with an approximate N40W direction; 4-5) The Santo Anastácio and Guapiara Faults both with a N60W direction, and 6) A local fault with N10E direction limited by the previous two faults.

A structural and stratigraphic trap was identified in Block 4 based on the structural high and contact between the Irati Formation rocks and the overlaying mudstone-dominated Serra Alta and Teresina Formations (Figs. 9 and 10). In the Block 4 domain, there is no incidence of any other faults that could allow some possible CO_2 leakage. Within Block 4, the Irati Formation covers an area above 1,800 km² with an average thickness of 38 m, an average depth of 2,640 m, and an average distance of 920 m from the Botucatu Formation (Guarani Aquifer) base. Davies *et al* consider 588 m as the maximum distance for the propagation of fractures in hydraulic fracking processes, considering the thousands of fracture operations performed in the shales of Marcellus, Barnett, Eagle Ford, and other fields. [65] Therefore, the average distance of 920 m from the aquifer is safe. The immediate sequence of about 65 m in thickness overlying the Irati Formation is the Serra Alta Formation consisting of shales and mudstones.[47] The Serra Alta Formation has the Teresina Formation of about 685 m in thickness consisting of mudstones interlaminated with fine sandstones on its top. Therefore, the two (Serra Alta and Teresina) formations will provide a combined caprock with an average thickness of about 750 m.

Local 3D geological model

Two wells (1-TI-1-SP and the 2-TB-1-SP) are inside Block 4. The model indicates a CO_2 reservoir within Block 4 refining the Irati Formations domain (meshes), considering the previously defined Units A/B/C to H (Fig. 12), and a diabase dike that was intercepted by the well 1-TI-1-SP (from 2,854 to 3,140 m). The dike is interpreted as subvertical, trending N55W in the same direction of magnetic lineaments within the study location, based on the airborne magnetic survey images,[43] and also because it is the preferred direction for intrusions.[44] Therefore, the diabase dike divides Block 4 in two (Fig. 11). The site considered for CO_2 storage is on the eastern side of the diabase dike (Fig. 11). Thus, the study presents a potential CO_2 reservoir covering approximately 1,200 km², bounded by the Mogi Lineament to the north, the Guapiara Fault to the northeast, the diabase dike to the southwest, and a local N10E trending fault to the southeast.

LOCAL ASPECTS OF THE CO_2 RESERVOIR

Porosity and permeability

Table 1 shows the porosity (Φ) and permeability (K) calculated from well 2-TB-1-SP for the Irati Formation shale units. Porosity is estimated using sonic-derived values based on equations from literature.[66] The

values computed for porosity were used to predict the permeability of the layers based on the redefined equations for shale units.[66] The porosity of the shale Units A/B/C and F varies from 8.0 to 16.7%, and the permeability from 0.542 to 75.11 mD. While the porosity of the black shale Units E and H range from 6.1 to 9.2%, and permeability values range from 0.088 to 1.383 mD.

Geothermal gradient and temperature

Gomes [67] presented the geothermal gradient of 20.4 ºC/km with a standard deviation of 1.02 calculated through the bottom-hole temperature (BHT) method,[68] for the Irati Formation in the well 2-TB-1-SP. The geothermal gradient is suitable for CO_2 storage considering recommended range (below 30 ºC/km) based on existing atlases.[5, 58] Therefore, a reservoir at 2,640 m depth with a geothermal gradient of 20.4 ºC/km should have an average temperature of 53.8 ºC, which is also within the recommended (≥ 35 ºC) range.[58]

CAPACITY ESTIMATION AND CLASSIFICATION

Among the current CO_2 storage reservoir choices, the shale formations seem to have the best potential, especially the black shales with total organic content (TOC) above 2%.[69] The available TOC data of the Irati Formation shale at intervals within well 2-TB-1-SP varies from 0.52 to 9.62% (Table 2). Although the black shale Unit H presents higher TOC values (8.45 and 9.62%) compared to Unit E (0.52 to 7.36%), the study considered reservoir CO_2 storage capacity estimation of Unit E due to its higher thickness (20.00 m for Unit E against 2.00 m for Unit H) (Table 1 and Fig. 3).

The study considered the DOE NETL equation for shales to estimate the CO_2 capacity of the reservoir.[69] According to Azenkeng *et al*, there are several challenges regarding storage capacity estimation based on shale reservoirs.[70] Factors that control the CO_2 storage in organic-rich shales are matrix pore spaces, and natural and induced fractures, which are not easily differentiated.[70] Table 3 summarizes the variables engaged for the storage capacity estimation in the organic-rich shale Unit E of Irati Formation within Block 4. The calculated porosity of 6.1% based on well 2-TB-1-SP within the Unit E (Table 1) connotes the natural fractures and pore spaces. The approach assumed for this initial assessment of the Irati Formation shale reservoir was quite conservative. The study engaged the CO_2 density of 842.3 kg/m^3 at supercritical conditions considering the geothermal gradient of 20.4 ºC/km,[67] an average depth of 2.640 m from the well 2-TB-1-SP, and an assumed hydrostatic gradient of 10.7 kPa/m for capacity estimation.

Weniger *et al* performed high-pressure experimental sorption isotherms with CO_2 at 45 °C on shale samples from the Irati Formation.[35] The Langmuir sorption model is a limiting model for low pressures, Weniger *et al* applied a modified Langmuir model with an average Langmuir pressure of 15,81 Mpa for the Irati Formation shale samples.[35] These authors also recognize a linear correlation between TOC (wt.%) data and the sorption capacities of CO_2, in agreement with literature results achieved for the Kentucky and the Marcellus Shale.[71, 72] The CO_2 sorbed mass was calculated using the gradient of 10.7

kPa/m at average depth of 2.640 m, and weighted average TOC of 3.2%, both from well 2-TB-1-SP, using the correlation equations from Weniger *et al*.[35]

The volume was directly obtained from the 3D solid of the black shale Unit E from the 3D implicit geological model (Table 3). The volume estimation did not directly involve the area efficiency factor (E_A) and thickness efficiency factor (E_h) because of some previously considered legal surface and structural (limiting faults) constraints in the site selection process. Although almost all geological parameters (porosity, temperature, thickness, and TOC) come from a single exploration well (2-TB-1-SP), the volume has a considerable level of reliability based on the constructed 3D geological model, which also considers the lithology data of all other 31 wells, geological mapping, topography, and local and regional structures.

The two efficiency factors from DOE NETL's equation (E_Φ and E_s) were assumed from the simulations of Myshakin *et al*,[73] contemplating 60 years of CO_2 injection. Considering the most conservative parameters of P_{10} probability values of 0.15 for E_Φ, and 0.11 for E_s, Unit E shows a CO_2 storage capacity of 1.85 billion tons (Table 3). Considering the P_{90} probability values of 0.36 for , and of 0.24 for from Myshakin *et al*,[73] the total capacity would be 4.44 billion tons. For comparison with other organic-rich shale formations, in the Devonian shale in Kentucky, a capacity of 27.7 Gt was estimated at least 304 m deep and 15 m thick,[71] while in the Marcellus Shale a total theoretical capacity of 171.2 Gt was estimated for a depth greater than 915 m.[72]

Bachu *et al* proposed a classification considering technical and economic aspects in four categories: theoretical, effective, practical, and matched capacity, according to a gradual level of uncertainty in storage potential.[74] The present study is the initial assessment of the shales of Irati Formation as a CO_2 reservoir considering the basic geological aspects while aiming to provide the basis for future studies addressing technical parameters (e.g. injection, wettability, capillary pressure, relative permeability, geochemical reactions) and involving numerical models. We assume a Theoretical classification even if a few associated parameters, such as seal, depth, geothermal gradient, temperature, and distance to aquifers are well defined. Although these parameters may not vary with the progress of the research, there is a need for an explicitly detailed definition to reduce the associated uncertainties involving CO_2 storage within the Irati Formation.

Discussion

Site selection

Table 4 presents the parameters considered for site selection and evaluation of potential CO_2 reservoirs. Within the study location, the conditions (low seismicity, absence of fold belts, uniform stratigraphy, high seal/overburden integrity, and the presence of reservoir-seal pairs) considered for CO_2 storage conform to the required standards based on existing atlases.[5, 58, 75] Therefore, the study location presents good CO_2

storage potentials within the black shale repositories. Although the research considered limitations involving the Paraná state legislation that prevents hydraulic fracturing within the region, it is pertinent to address the associated social and environmental factors.[76]

The 3D implicit modeling is more robust and has better representativeness of the structure and geology than other surface-based methods, improving the modeling accuracy.[14, 77] The methodology of implicit modeling aided to build thematic models based on the depth and thickness of the Irati Formation sequence. The models enhance quick interpretations, and the evaluation involving the distance to protect groundwater (Guarani Aquifer system) proves satisfactory and with fast results of easy interpretation (Figs. 5, 6, and 7). The presented technique applies to other regions especially at the CO_2 storage Site Selection stage. The 3D structural model divided the study area into seven fault blocks and defined a structural high (based on Block 4) to indicate a combined structural and stratigraphic trap (Figs. 8, 9, and 10). These geological aspects of the selected site are favorable for CO_2 storage. The siltstones of Serra Alta and Teresina formations occur on the vertical and horizontal scales to serve as seals and traps for the Irati Formation shale units, preventing post-CO_2 storage leakages. The study incorporated data from wellbores, surface, regional geological and structural mapping to construct the 3D geological model. The evaluation (e.g. seismic interpretation) involving fault plane orientation and distribution with other associated structures not visible in the current work scale is pertinent to describe the detailed structural framework.

Reservoir potential

Considering the CO_2 reservoir located in the black shale Unit E, there are 15 power plants within a radius of 75 km with a total installed capacity of 562 MW. 13 of these power plants depend on biomass (mainly sugarcane bagasse), and the other two power plants use diesel fuel.[78] There are 81 power plants total capacity of 1,625 MW within a radius of 150 km around the shale Unit E. A biomass power plant with 600 MW capacity emits on average 3.5 million tons of CO_2 per year, according to 2018 base year data from the United States Environmental Protection Agency.[79] The theoretical capacity of 1.85 Gt of CO_2 storage in the Irati Formation organic-rich shale would account for the equivalent production of 500 years of only the 75 km radius power plants. Alternatively, applying a simple regression, the CO_2 site location could support up to five times more than the current capacity considering a regional industrial park installation in a long-term horizon of about 68 years, taking into account also the location and the privileged infrastructure of the region.

The CO_2 geological storage in organic-rich shales has been considered a promissory way to mitigate greenhouse gas emissions. The study includes the advantages commonly pointed out in CO_2 storage sites around the world as the volumetric spatial continuity and geological extension, adequate depth, and potential for methane recovery in the Irati shales. The research presents the theoretical CO_2 storage capacity of the reservoir considering free pore spaces and stratigraphic traps. Furthermore, limited petrophysical data is a challenge. The study also estimates de CO_2 trapping by adsorption based on the

limited available literature concerning the Irati Formation. Therefore, future studies should account for associated challenges such as low permeability, matrix porosity, and geological heterogeneity within the Irati Formation shales.

Concluding Remarks

1. The Paraná Basin in Southeastern Brazil meets most of the requirements for CO_2 storage base on international best practices. These conditions include the low seismicity, the absence of fold belt, uniform stratigraphy, the absence of complex lateral variations, and the presence of reservoir-seal pairs in multi-layered systems.

2. The application of 3D implicit modeling provided a fast approach via the thematic models to delimitate potential CO_2 reservoirs based on the reservoir depth, thickness, structural geology, and distance to protect groundwater (aquifer) proves satisfactory.

3. The Irati Formation was locally subdivided into two shale units (Units A/B/C and F), two limestone units (Units D and G), and two black shale units (Units E and H) in a three-dimensional ambient. The black shale Unit E was evaluated for CO_2 geological storage.

4. The organic-rich shale Unit E within Block 4 of the Irati Formation has a theoretical CO_2 reservoir capacity of 1.85 Gt of CO_2, assuming a CCS project with CO_2 injection at supercritical conditions through hydraulic fracturing.

5. The results provide the basis of subsequent studies involving mineral characterization of each geological unit of Irati Formation and numerical simulations.

Declarations

ACKNOWLEDGMENTS

We gratefully acknowledge the support of the Research Centre for Gas Innovation (RCGI), hosted by the Universidade de São Paulo (USP), Shell Brasil, Fundação de Amparo à Pesquisa do Estado de São Paulo (FAPESP), and the strategic importance of the support given by Agência Nacional do Petróleo, Gás Natural e Biocombustíveis (ANP) through the R&D levy regulation, and for providing exploration well data. The authors are also grateful to Seequent Limited for providing the Leapfrog Geothermal academic license.

References

1. IEA. Global energy & CO_2 status report 2019. Paris. (2019).

2. Azevedo TR, Costa Junior C, Brandão Junior A, Cremer MdS, Piatto M, Tsai DS, et al. SEEG initiative estimates of Brazilian greenhouse gas emissions from 1970 to 2015. Scientific Data 5:180045 (2018).

3. SEEG. Sistema de Estimativas de Emissões e Remoções de Gases de Efeito Estufa: Observatório do Clima; 2020 [Available from: http://seeg.eco.br/.

4. Bachu S. Sequestration of CO_2 in geological media: criteria and approach for site selection in response to climate change. Energy Conversion and Management 41:953-970 (2000).

5. Miocic JM, Gilfillan SMV, Roberts JJ, Edlmann K, McDermott CI, Haszeldine RS. Controls on CO2 storage security in natural reservoirs and implications for CO2 storage site selection. International Journal of Greenhouse Gas Control 51:118-125 (2016).

6. IPCC. Intergovernmental panel on climate change special report on carbon dioxide capture and storage. Cambridge, UK and New York, USA: Intergovernmental Panel on Climate Change. (2005).

7. Orr FM. Onshore Geologic Storage of CO_2. Science 325:1656 (2009).

8. Zhang D, Song J. Mechanisms for Geological Carbon Sequestration. Procedia IUTAM 10:319-327 (2014).

9. Raza A, Gholami R, Rezaee R, Rasouli V, Rabiei M. Significant aspects of carbon capture and storage – A review. Petroleum 5:335-340 (2019).

10. Bradshaw J, Bachu S, Bonijoly D, Burruss R, Holloway S, Christensen NP, et al. CO_2 storage capacity estimation: Issues and development of standards. International Journal of Greenhouse Gas Control 1:62-68 (2007).

11. Godec ML, Jonsson H, Basava-Reddi L. Potential global implications of gas production from shales and coal for geological CO_2 storage. Energy Procedia 37:6656-6666 (2013).

12. Khosrokhavar R, Griffiths S, Wolf K-H. Shale gas formations and their potential for carbon storage: opportunities and outlook. Environmental Processes 1:595-611 (2014).

13. Boosari SSH, Aybar U, Eshkalak MO. Carbon dioxide storage and sequestration in unconventional shale reservoirs. Journal of Geoscience and Environment Protection 3:7-15 (2015).

14. Cowan EJ, Beatson RK, Ross HJ, Fright WR, McLennan TJ, Evans TR, et al., editors. Practical implicit geological modelling. Fifth international mining geology conference; Bendigo, Victoria: Australian Institute of Mining and Metallurgy (2003).

15. Cowan EJ, Beatson RK, Fright WR, McLennan TJ, Mitchell TJ, editors. Rapid geological modelling. Applied Structural Geology for Mineral International Symposium; Kalgoorlie. (2002).

16. Birch C. New systems for geological modelling - black box or best practice? Journal of the Southern African Institute of Mining and Metallurgy 114:993-1000 (2014).

17. Jessell M, Aillères L, De Kemp E, Lindsay M, Wellmann JF, Hillier M, et al. Next generation three-dimensional geologic modeling and inversion. Society of Economic Geologists Special Publication 18:261-272 (2014).

18. Stoch B, Anthonissen CJ, McCall MJ, Basson IJ, Deacon J, Cloete E, et al. 3D implicit modeling of the Sishen Mine: new resolution of the geometry and origin of Fe mineralization. Mineralium Deposita 53:835-853 (2018).

19. Kampmann TC, Stephens MB, Weihed P. 3D modelling and sheath folding at the Falun pyritic Zn-Pb-Cu-(Au-Ag) sulphide deposit and implications for exploration in a 1.9 Ga ore district, Fennoscandian Shield, Sweden. Mineralium Deposita 51:665-680 (2016).

20. Schetselaar E, Pehrsson S, Devine C, Lafrance B, White D, Malinowski M. 3-D geologic modeling in the Flin Flon mining district, Trans-Hudson orogen, Canada: Evidence for polyphase imbrication of the Flin Flon-777-Callinan volcanogenic massive sulfide ore system. Econ Geol 111:877-901 (2016).

21. de Oliveira SB, Johnson CA, Juliani C, Monteiro LVS, Leach DL, Caran MGN. Geology and genesis of the Shalipayco evaporite-related Mississippi Valley-type Zn–Pb deposit, Central Peru: 3D geological modeling and C–O–S–Sr isotope constraints. Mineralium Deposita (2021).

22. Vollgger SA, Cruden AR, Ailleres L, Cowan EJ. Regional dome evolution and its control on ore-grade distribution: Insights from 3D implicit modelling of the Navachab gold deposit, Namibia. Ore Geology Reviews 69:268-284 (2015).

23. Naranjo A, Horner J, Jahoda R, Diamond LW, Castro A, Uribe A, et al. La Colosa Au Porphyry Deposit, Colombia: Mineralization Styles, Structural Controls, and Age Constraints. Econ Geol 113:553-578 (2018).

24. Cowan EJ. Deposit-scale structural architecture of the Sigma-Lamaque gold deposit, Canada—insights from a newly proposed 3D method for assessing structural controls from drill hole data. Mineralium Deposita 55:217-240 (2020).

25. Alcaraz S, Chamberfort I, Pearson R, Cantwell A, editors. An integrated approach to 3-D modelling to better understand geothermal reservoirs. Proceedings World Geothermal Congress; 2015; Melbourne, Australia. (2015).

26. Kaufmann O, Martin T. 3D geological modelling from boreholes, cross-sections and geological maps, application over former natural gas storages in coal mines. Computers & Geosciences 34:278-290 (2008).

27. Douglass J, Kelly B, editors. 3D geological modelling and carbon storage potential of the Sydney Basin. Thirty Seventh Symposium on the Geology of the Sydney Basin; May 6-7, 2010; Pokolbin, Australia. (2010).

28. Monaghan A, Ford J, Milodowski A, McInroy D, Pharaoh T, Rushton J, et al. New insights from 3D geological models at analogue CO_2 storage sites in Lincolnshire and eastern Scotland, UK. Proc Yorkshire Geol Soc 59:53 (2012).

29. Alcalde J, Marzán I, Saura E, Martí D, Ayarza P, Juhlin C, et al. 3D geological characterization of the Hontomín CO2 storage site, Spain: Multidisciplinary approach from seismic, well-log and regional data. Tectonophysics 627:6-25 (2014).

30. Lech ME, Jorgensen DC, Southby C, Wang L, Nguyen V, Borissova I, et al. Palaeogeographic mapping to understand the hydrocarbon and CO2 storage potential of the post-rift Warnbro Group, offshore Vlaming Sub-basin, southern Perth Basin, Australia. Marine and Petroleum Geology 77:1206-1226 (2016).

31. Mediato JF, García-Crespo J, Izquierdo E, García-Lobón JL, Ayala C, Pueyo EL, et al. Three-dimensional Reconstruction of the Caspe Geological Structure (Spain) for Evaluation as a Potential CO2 Storage Site. Energy Procedia 114:4486-4493 (2017).

32. Shogenov K, Forlin E, Shogenova A. 3D Geological and Petrophysical Numerical Models of E6 Structure for CO2 Storage in the Baltic Sea. Energy Procedia 114:3564-3571 (2017).

33. Vo Thanh H, Sugai Y, Nguele R, Sasaki K. Integrated workflow in 3D geological model construction for evaluation of CO2 storage capacity of a fractured basement reservoir in Cuu Long Basin, Vietnam. International Journal of Greenhouse Gas Control 90:102826 (2019).

34. Zhong Z, Carr TR. Geostatistical 3D geological model construction to estimate the capacity of commercial scale injection and storage of CO2 in Jacksonburg-Stringtown oil field, West Virginia, USA. International Journal of Greenhouse Gas Control 80:61-75 (2019).

35. Weniger P, Kalkreuth W, Busch A, Krooss BM. High-pressure methane and carbon dioxide sorption on coal and shale samples from the Paraná Basin, Brazil. International Journal of Coal Geology 84:190-205 (2010).

36. Lima Vd, Einloft S, Ketzer JM, Jullien M, Bildstein O, Petronin J-C. CO_2 Geological storage in saline aquifers: Paraná Basin caprock and reservoir chemical reactivity. Energy Procedia 4:5377-5384 (2011).

37. Rockett GC, Machado CX, Ketzer JMM, Centeno CI. The CARBMAP project: Matching CO2 sources and geological sinks in Brazil using geographic information system. Energy Procedia 4:2764-2771 (2011).

38. Ketzer JM, Iglesias R, Einloft S, Dullius J, Ligabue R, de Lima V. Water–rock–CO2 interactions in saline aquifers aimed for carbon dioxide storage: Experimental and numerical modeling studies of the Rio Bonito Formation (Permian), southern Brazil. Applied Geochemistry 24:760-767 (2009).

39. Machado CX, Rockett GC, Ketzer JMM. Brazilian renewable carbon capture and geological storage map: Possibilities for the Paraná Basin. Energy Procedia 37:6105-6111 (2013).

40. Dalla Vecchia F, dos Santos VHJM, Schütz MK, Ponzi GGD, Stepanha ASdGe, Malfatti CdF, et al. Wellbore integrity in a saline aquifer: Experimental steel-cement interface degradation under supercritical CO2 conditions representative of Brazil's Parana basin. International Journal of Greenhouse Gas Control 98:103077 (2020).

41. Ketzer JMM, Machado CX, Rockett GC, Iglesias RS. Atlas brasileiro de captura e armazenamento geológico de CO_2. Porto Alegre: EDIPUCRS; 2016. 95 p.

42. Goodman A, Hakala A, Bromhal G, Deel D, Rodosta T, Frailey S, et al. U.S. DOE methodology for the development of geologic storage potential for carbon dioxide at the national and regional scale. International Journal of Greenhouse Gas Control 5:952-965 (2011).

43. Lopes RC, Peruffo N, Sachs LLB, Silva VA, I.H. B. Folha SF 22 Paranapanema. In: Schobbenhaus C, Gonçalves JH, Santos JOS, Abram MB, Leão Neto R, Matos GMM, et al., editors. Carta Geológica do Brasil ao Milionémo, Sistema de Informações Geográficas Programa Geologia do Brasil. Brasilia: CPRM.(2004).

44. Zalán PV, Wolff S, Astolfi MAM, Vieira IS, Concelcao JCJ, Appi VT, et al. The Parana Basin, Brazil: Chapter 33: Part II. Selected Analog Interior Cratonic Basins: Analog Basins. In: Leighton MW, Kolata DR, Oltz DF, Eidel JJ, editors. Interior Cratonic Basins. 51. Tulsa, USA: AAPG; p. 681-708.(1990).

45. Milani EJ, Faccini UF, Scherer CM, Araújo LMd, Cupertino JA. Sequences and stratigraphic hierarchy of the Paraná Basin (Ordovician to Cretaceous), southern Brazil. Boletim IG-USP 29:125-173 (1998).

46. Thomaz Filho A, Mizusaki AMP, Antonioli L. Magmatism and petroleum exploration in the Brazilian Paleozoic basins. Marine and Petroleum Geology 25:143-151 (2008).

47. Holz M, França AB, Souza PA, Iannuzzi R, Rohn R. A stratigraphic chart of the Late Carboniferous/Permian succession of the eastern border of the Paraná Basin, Brazil, South America. Journal of South American Earth Sciences 29:381-399 (2010).

48. Euzébio RS, Reis DES, Brito M, Bergamaschi S, Martins MVA, Rodrigues R. Oil generation potential assessment and paleoenvironmental interpretation of Irati Formation (Lower Permian) in northwestern of Paraná Basin (Brazil). Journal of Sedimentary Environments 1:261-274 (2016).

49. Reis DES, Rodrigues R, Moldowan JM, Jones CM, Brito M, Costa Cavalcante D, et al. Biomarkers stratigraphy of Irati Formation (Lower Permian) in the southern portion of Paraná Basin (Brazil). Marine and Petroleum Geology 95:110-138 (2018).

50. Alferes C, Rodrigues R, Pereira E. Geoquímica orgânica aplicada à Formação Irati, na área de São Mateus do Sul (PR), Brasil. Geochimica Brasiliensis 25:47-54 (2011).

51. Iglesias RS, Ketzer JM, Melo CL, Heemann R, Machado CX. Carbon capture and geological storage in Brazil: an overview. Greenhouse Gases: Science and Technology 5:119-130 (2015).

52. Ramos KN, Petry PM, de Medeiros Costa HK. ATUALIZAÇÕES DA EXPLORAÇÃO DE GÁS NÃO CONVENCIONAL NO BRASIL. Revista Gestão & Sustentabilidade Ambiental 9:237-258 (2020).

53. Lenhard LG, Andersen SM, Coimbra-Araújo CH. Energy-Environmental Implications Of Shale Gas Exploration In Paraná Hydrological Basin, Brazil. Renewable and Sustainable Energy Reviews 90:56-69 (2018).

54. Costa HKM, Musarra RMLM. Law sources and CCS (carbon capture and storage) regulation in Brazil. International Journal of Advanced Engineering Research and Science 7:196-201 (2020).

55. Almeida JRL, Vasconcellos Rocha H, Medeiros Costa H, Santos EM, Rodrigues CF, Sousa MJL. Analysis of civil liability regarding CCS: The Brazilian case. Modern Environmental Science and Engineering 3:382-395 (2017).

56. da Silva FTF, Carvalho FM, Corrêa JLG, Merschmann PRdC, Tagomori IS, Szklo A, et al. CO_2 capture in ethanol distilleries in Brazil: Designing the optimum carbon transportation network by integrating hubs, pipelines and trucks. International Journal of Greenhouse Gas Control 71:168-183 (2018).

57. Milani EJ, Thomaz Filho A. Sedimentary basins of South America. In: Cordani UG, Milani EJ, Thomaz Filho A, Campos DA, editors. Tectonic Evolution of South America. 31. Rio de Janeiro, Brazil: In-Fólio Produção Editorial, ; p. 389-449.(2000).

58. IEA-GHG. IEA greenhouse gas R&D programme: CCS Site characterisation criteria. Cheltenham, United Kingdom. (2009).

59. Berrocal J, Fernandes C, Bassini A, Barbosa JR. Earthquake hazard assessment in southeastern Brazil. Geofísica Internacional 35:257-272 (1996).

60. Silva FdP, Kiang CH, Caetano-Chang MR. Hidroestratigrafia do Grupo Bauru (K) no Estado de São Paulo. Águas Subterrâneas 19:18 (2005).

61. Gilboa Y, Mero F, Mariano IB. The Botucatu aquifer of South America, model of an untapped continental aquifer. J Hydrol 29:165-179 (1976).

62. Araújo LM, França AB, Potter PE. Hydrogeology of the Mercosul aquifer system in the Paraná and Chaco-Paraná Basins, South America, and comparison with the Navajo-Nugget aquifer system, USA. Hydrogeol J 7:317-336 (1999).

63. Milani EJ, Ramos VA. Orogenias paleozóicas no domínio sul-ocidental do Gondwana e os ciclos de subsidência da Bacia do Paraná. Revista Brasileira de Geociências 28:473-484 (1998).

64. Etheridge MA, Branson JC, Stuart-Smith PG. Extensional basin-forming structures in Bass Strait and their importance for hydrocarbon exploration. The APPEA Journal 25:344-361 (1985).

65. Davies RJ, Mathias SA, Moss J, Hustoft S, Newport L. Hydraulic fractures: How far can they go? Marine and Petroleum Geology 37:1-6 (2012).

66. Richardson MA-A, Taioli F. Hydrocarbon viability prediction of some selected reservoirs in Osland Oil and gas field, Offshore Niger Delta, Nigeria. Marine and Petroleum Geology 100:195-203 (2019).

67. Gomes AJL. Avaliação de recursos geotermais da Bacia do Paraná. Rio de Janeiro: Observatório Nacional; 2009.

68. Carvalho HDS, Vacquier V. Method for determining terrestrial heat flow in oil fields. Geophysics 42:584-593 (1977).

69. Levine JS, Fukai I, Soeder DJ, Bromhal G, Dilmore RM, Guthrie GD, et al. U.S. DOE NETL methodology for estimating the prospective CO2 storage resource of shales at the national and regional scale. International Journal of Greenhouse Gas Control 51:81-94 (2016).

70. Azenkeng A, Mibeck BAF, Kurz BA, Gorecki CD, Myshakin EM, Goodman AL, et al. An image-based equation for estimating the prospective CO2 storage resource of organic-rich shale formations. International Journal of Greenhouse Gas Control 98:103038 (2020).

71. Nuttal BC, Eble C, Bustin RM, Drahovzal JA. Analysis of Devonian black shales in kentucky for potential carbon dioxide sequestration and enhanced natural gas production. In: Rubin ES, Keith DW, Gilboy CF, Wilson M, Morris T, Gale J, et al., editors. Greenhouse Gas Control Technologies 7. Oxford: Elsevier Science Ltd; p. 2225-2228.(2005).

72. Godec M, Koperna G, Petrusak R, Oudinot A. Potential for enhanced gas recovery and CO2 storage in the Marcellus Shale in the Eastern United States. International Journal of Coal Geology 118:95-104 (2013).

73. Myshakin EM, Singh H, Sanguinito S, Bromhal G, Goodman AL. Numerical estimations of storage efficiency for the prospective CO2 storage resource of shales. International Journal of Greenhouse Gas Control 76:24-31 (2018).

74. Bachu S, Bonijoly D, Bradshaw J, Burruss R, Holloway S, Christensen NP, et al. CO_2 storage capacity estimation: Methodology and gaps. International Journal of Greenhouse Gas Control 1:430-443 (2007).

75. Smith M, Campbell D, Mackay E, Polson D. CO_2 aquifer storage site evaluation and monitoring: Understanding the challenges of CO_2 storage: results of the CASSEM project. Heriot-Watt University, Edimburgh: Scottish Carbon Capture and Storage (SCCS); 2011.

76. Ciotta M, Peyerl D, Barrozo L, Sant Anna L, Moutinho dos Santos E, Bermann C, et al. An overview of carbon capture and storage atlases around the world. Environ Geosci 27:1-8 (2020).

77. Wellmann F, Caumon G. Chapter One - 3-D Structural geological models: Concepts, methods, and uncertainties. In: Schmelzbach C, editor. Adv Geophys. 59: Elsevier; p. 1-121.(2018).

78. ANEEL-SIGEL. Data base of the Brazilian Power Sector-SIGEL Rio de Janeiro2020 [Available from: https://sigel.aneel.gov.br/Down/.

79. EPA. Emissions & generation resource integrated database (eGRID) Washington, DC: United States Environmental Protection Agency; 2020 [Available from: https://www.epa.gov/energy/egrid,.

Tables

Table 1. Rock type, thickness, porosity (Φ), and permeability (K) data for shale units of Irati Formation in the 2-TB-1-SP well.

Unit	Rock type	Thickness (m)	Φ	K (mD)
H	Black shale	2.00	0.092	1.383
F	Shale	1.00	0.080	0.542
E	Black shale	20.0	0.061	0.088
A/B/C	Shale	7.00	0.167	75.11

Table 2. Total organic carbon (TOC wt.%) data on the Irati Formation intervals in the well 2-TB-1-SP, with the geological unit subdivision of this study.

Top	Bottom	Rock type	Unit	TOC wt.%
2,618.94	2,619.94	Black shale	H	8.45
2,620.00	2,621.00	Black shale	H	9.62
2,622.94	2,623.94	Limestone	G	2.02
2,623.94	2,624.94	Shale	F	1.44
2,624.94	2,625.95	Black shale	E	7.36
2,628.32	2,629.32	Black shale	E	7.26
2,631.32	2,632.32	Black shale	E	4.53
2,632.32	2,633.42	Black shale	E	2.88
2,633.42	2,633.82	Black shale	E	5.03
2,633.82	2,635.32	Black shale	E	2.45
2,635.32	2,636.32	Black shale	E	0.52
2,637.32	2,637.90	Black shale	E	1.15
2,640.00	2,646.00	Black shale	E	2.25
2,649.00	2,652.00	Limestone	D	1.51
2,653.40	2,654.40	Shale	A/B/C	0.19
2,656.28	2,657.28	Shale	A/B/C	0.28

Table 3. Theoretical CO_2 storage for the black shale Unit E of the Irati Formation.

Symbol	Unit	Parameters	Value
v	m^3	volume	23,914,000,000
Φ	%	porosity	6.1%
ρ_{CO2}	kg/m^3	CO_2 density at reservoir conditions	842.3
ρs_{CO2}	kg/m^3	mass of CO_2 sorbed per unit volume of solid rock	0.31
E_Φ	%	free phase storage efficiency factor	0.15%
E_s	%	sorption efficiency factor	0.11%
M_{CO2}	Gt	mass of CO_2	1.85

Table 4. Site selection criteria for geological CO_2 storage and our study results.

Criterion	Eliminatory or unfavourable	Preferred or Favourable	Reference	This study
Reservoir-seal pairs; extensive and competent barrier to vertical flow	Poor, discontinuous, faulted and/or breached	Intermediate and excellent; many pairs (multi-layered system)	IEA-GHG, 2009	Vertically sealing faults, multi-layered systems
	-	Vertically sealing faults, multi-layered systems	Miocic et al., 2016	
Stratigraphy	Complex lateral variation and complex connectivity	Uniform	Smith et al., 2011	Uniform
Located within fold belts	Yes	No	IEA-GHG, 2009	No
Seismicity	High	Moderate and less	IEA-GHG, 2009	Low
Depth	< 800 m or > 2,500 m	Between 1,000 and 2,500 m	Chadwick et al. 2008	Average depth 2,640 m
	< 750-800 m	> 800 m	IEA-GHG, 2009	
	< 800 m > 2,500m	> 800 m < 2,500 m	Smith et al., 2011	
	-	> 1,200 m	Miocic et al., 2016	
Thickness	< 20 m	> 50 m	Chadwick et al. 2008	Average thickness 20 m
	< 20 m	≥ 20 m	IEA-GHG, 2009	
Affecting protected groundwater quality	Yes	No	IEA-GHG, 2009	Distance of 920m to aquifer system
Faulting and fracturing intensity		Small or no faults	Chadwick et al. 2008	Minimal faulting, with trapping structure
	Extensive	Limited to moderate	IEA-GHG, 2009	
		Minimal faulting, with trapping structure	Smith et al., 2011	
Caprock thickness	< 20 m	> 100 m	Chadwick et al.	> 750 m (Serra Alta 64 m thick

			2008	+ Teresina Formations 690 m thick)
	< 10 m	≥ 10 m	IEA-GHG, 2009	
	< 20 m thick	> 100 m thick	Smith et al., 2011	
	-	> 150m	Miocic et al., 2016	
Lateral continuity of caprock	Lateral variations, faulted	Unfaulted (Uniform)	Chadwick et al. 2008	Unfaulted
Porosity	< 10%	> 20%	Chadwick et al. 2008	6.1%
	< 10%	≥ 10%	IEA-GHG, 2009	
	< 10%	> 20%	Smith et al., 2011	
Geothermal regime	Gradients ≥ 35 ºC/km and/or high surface temperature	Gradients < 35 ºC/km and low surface temperature	IEA-GHG, 2009	20.4 ºC/km
	-	Geo-thermal gradient of max. 30 ºC/km	Miocic et al., 2016	
Temperature	< 35 ºC	≥ 35 ºC	IEA-GHG, 2009	54 ºC
Total organic organic carbon	< 2.0%	≥ 2.0%	Goodman et al., 2014	3.15%
Well density	High	Low to moderate	IEA-GHG, 2009	Low
Proximity to powerplant	> 100 km	< 75 km	Smith et al., 2011	15 powerplants (562 MW) within a radius of 75 km
Total storage capacity	Total capacity estimated to be similar to or less than the total amount produced from the CO source	Total capacity estimated to be much larger than the total amount produced from the CO_2	Chadwick et al. 2008	Total capacity estimated to be much larger than the total amount produced from the CO_2

Figures

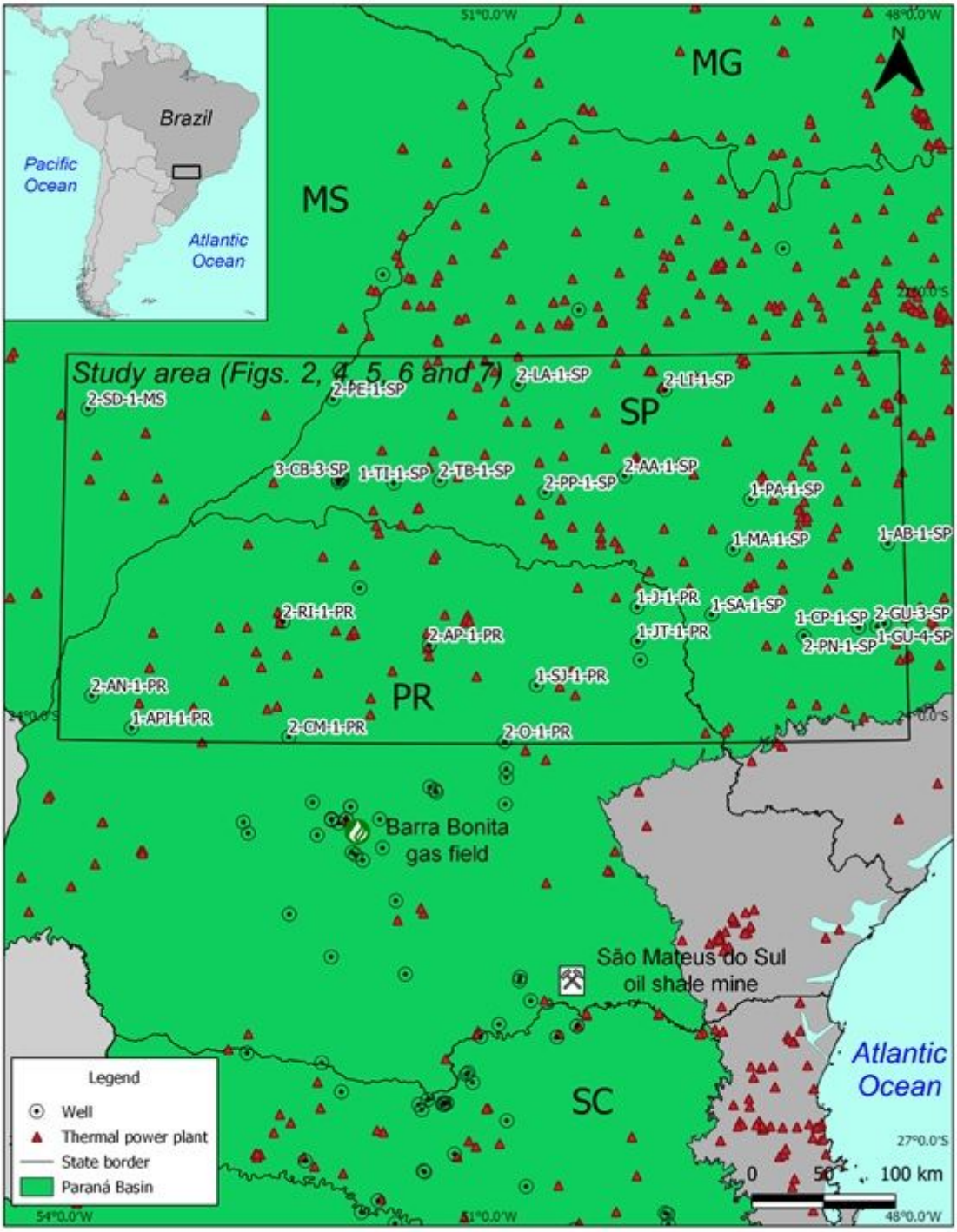

Figure 1

Location of wells, thermoelectric power plants, and the study area in the central Paraná Basin. Power plants' locations are from ANEEL-SIGEL 78. MG = Minas Gerais State, MS = Mato Grosso do Sul State, PR = Paraná State, SC = Santa Catarina State, SP = São Paulo State.

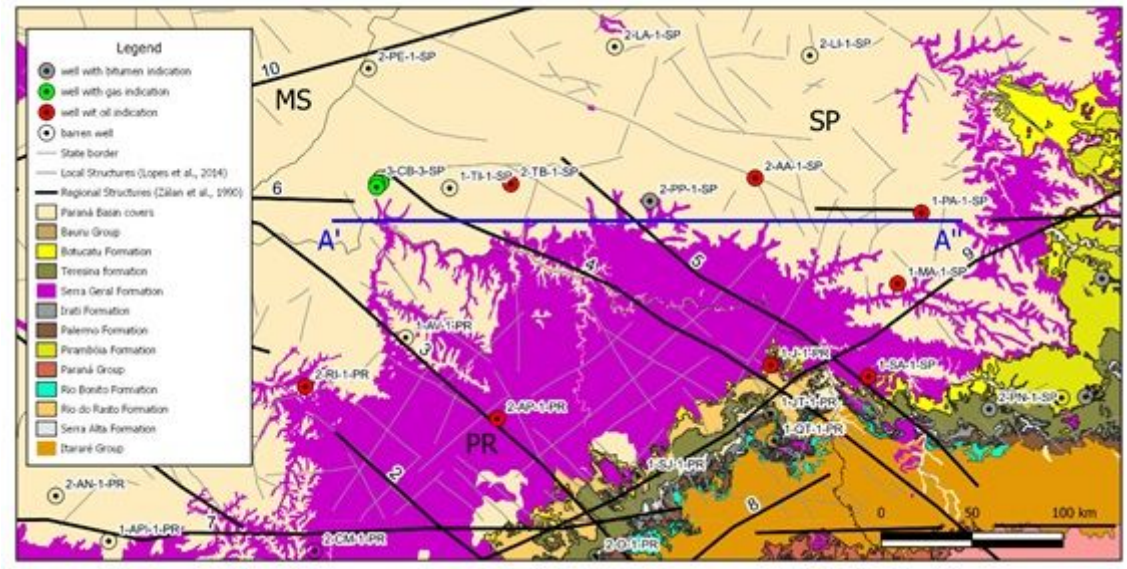

Figure 2

Geological map of the study area with local structures,43 and main regional structures.44 Location of the schematic geological section (A'-A") of Fig. 3. 1 - Cândido Fault, 2 - Curitiba Fault Zone, 3 - São Jerônimo Fault, 4 - Santo Anastácio Fault, 5 – Guapiara Fault Zone, 6 - Mogi Lineament, 7 - São Sebastião Lineament, 8 - Jacutinga Fault, 9 - Guaxupé Fault, 10 - Araçatuba Lineament.

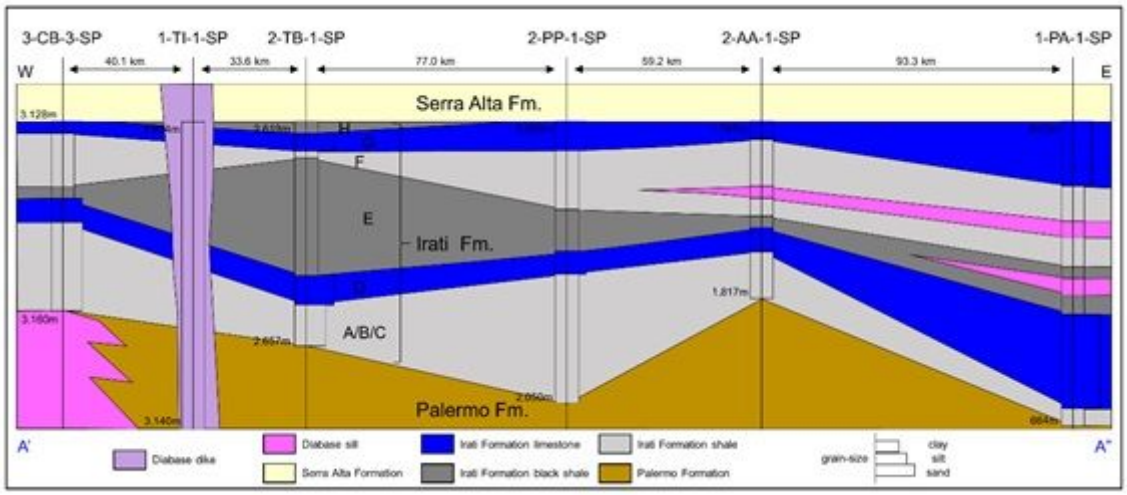

Figure 3

Schematic geological section of the Irati Formation with a local subdivision in six geological units: shale Unit A/B/C, limestone Unit D, black shale Unit E, shale Unit F, limestone Unit G, and black shale Unit H.

Figure 4

Intercalations of shale and limestone layers of Irati Formation in the Elba Quarry, Northwest of Paraná Basin.

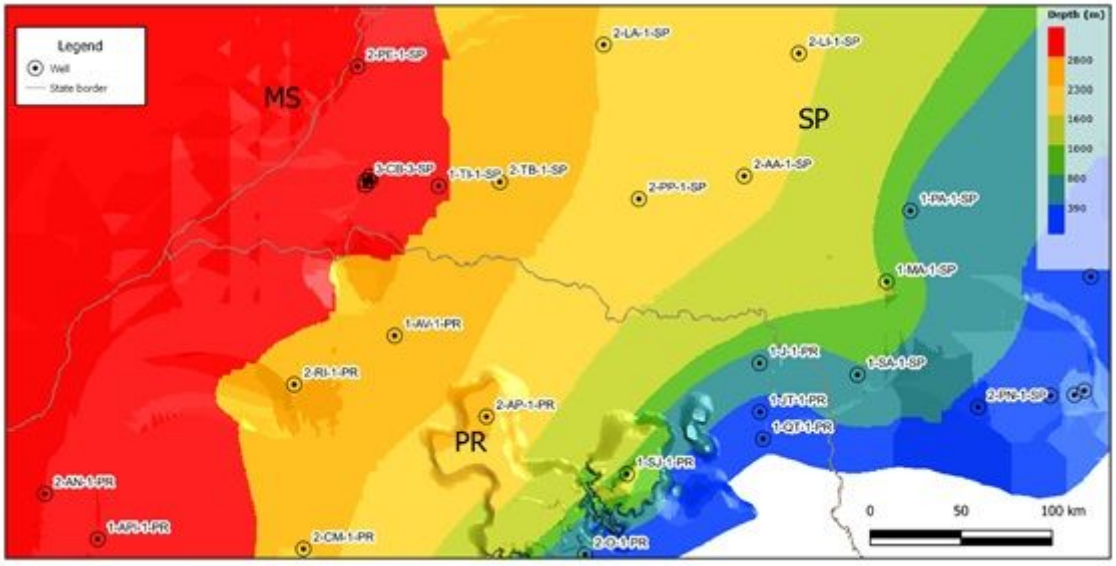

Figure 5

Plan view of the Irati Formation depth model in the study area.

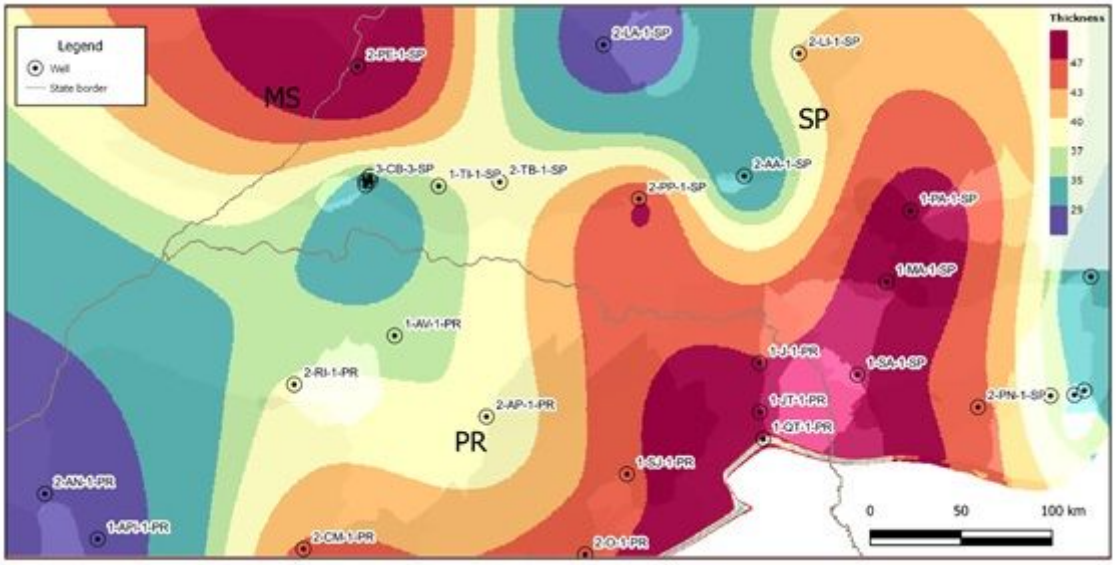

Figure 6

Plan view of the Irati Formation thickness model in the study area.

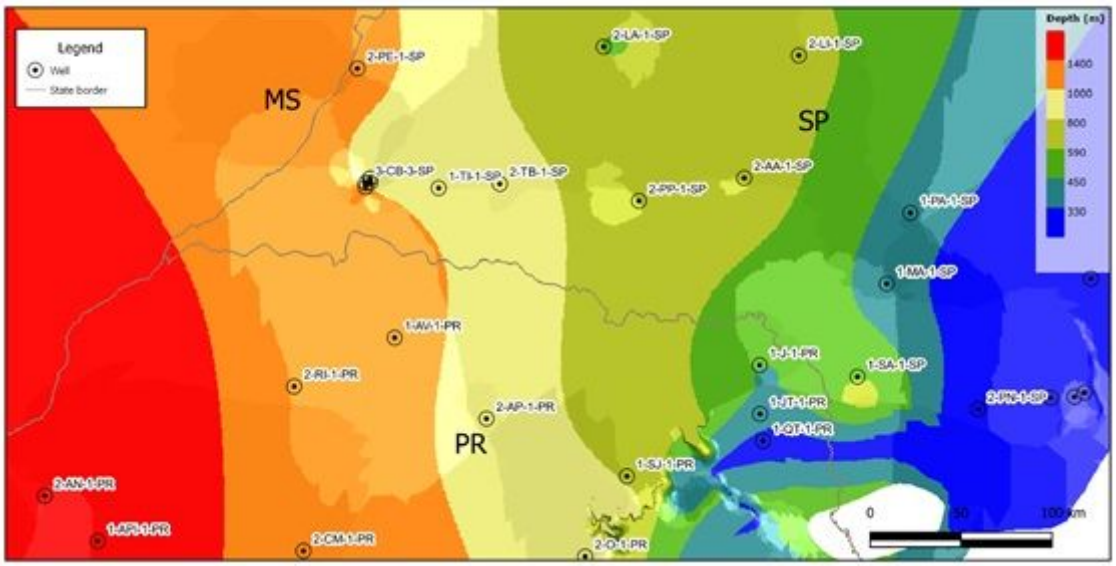

Figure 7

Plan view of the model of the distance from the top of the Irati Formation to the base of the Guarani Aquifer in the study area.

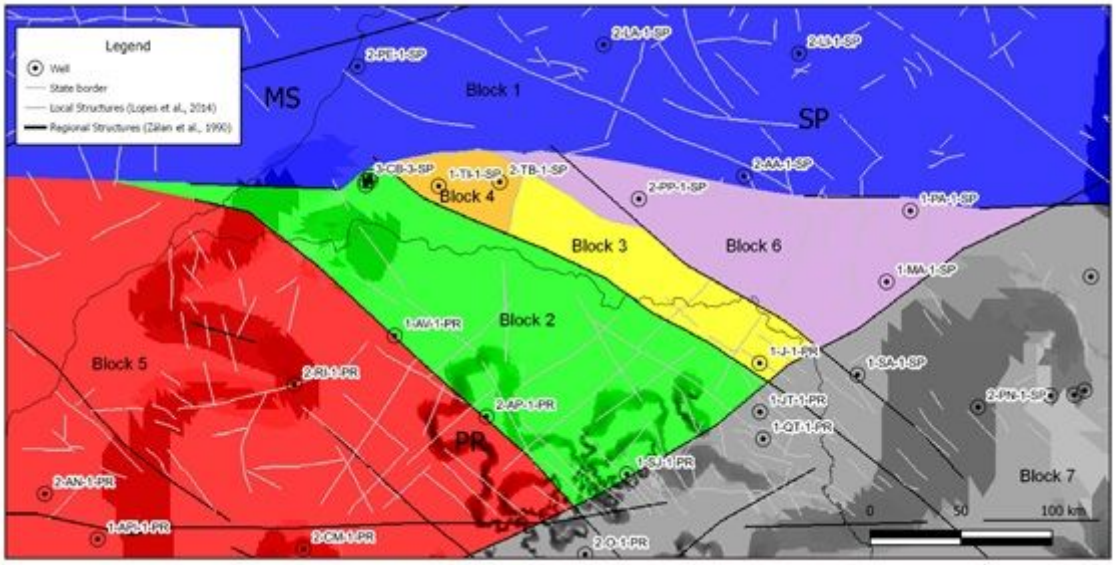

Figure 8

Plan view of the structural model showing the seven fault blocks defined by the main regional structures in the study area.

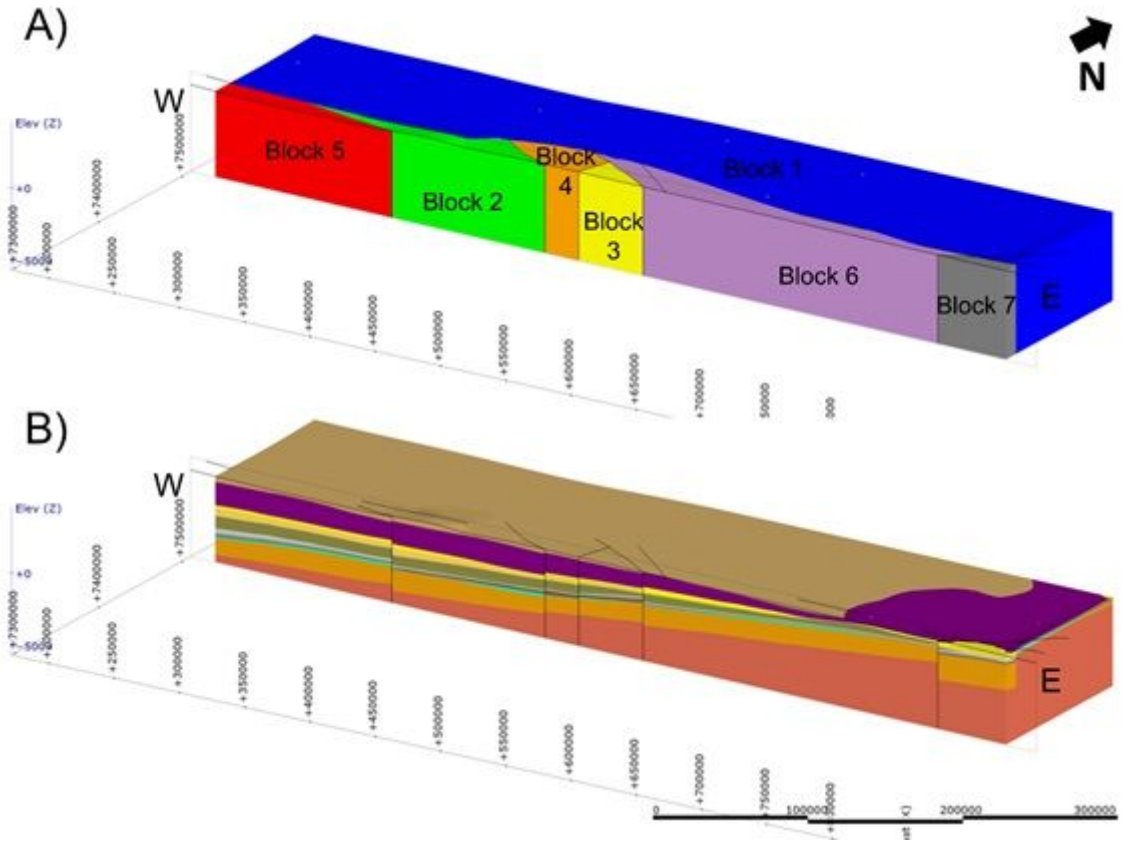

Figure 9

3D view with an E-W slice. A) Structural fault blocks. B) Structural geological model. The legend color is the same as in Fig. 2. Vertical scale = 10x.

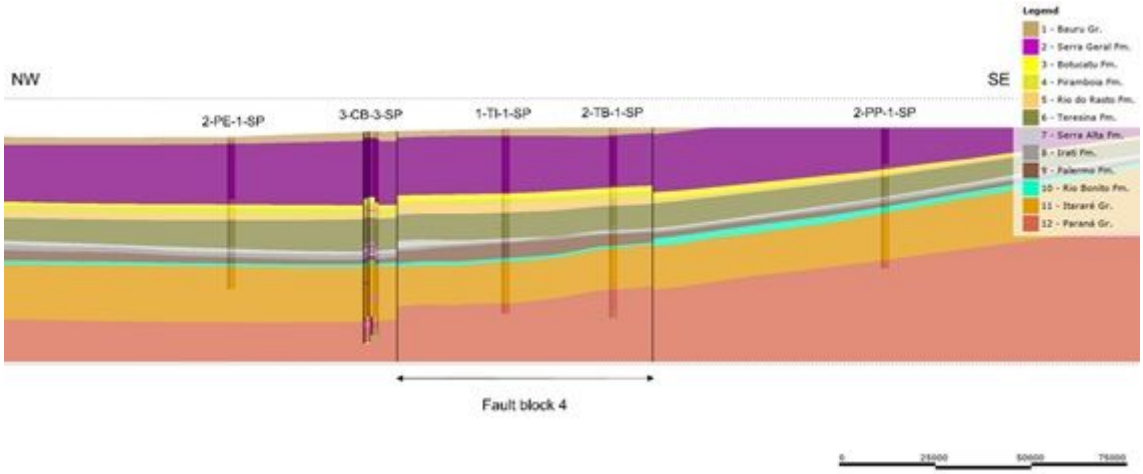

Figure 10

NW-SE section view of the 3D structural and geological modeling highlighting the Fault Block 4 as a structural high. Vertical scale = 10x.

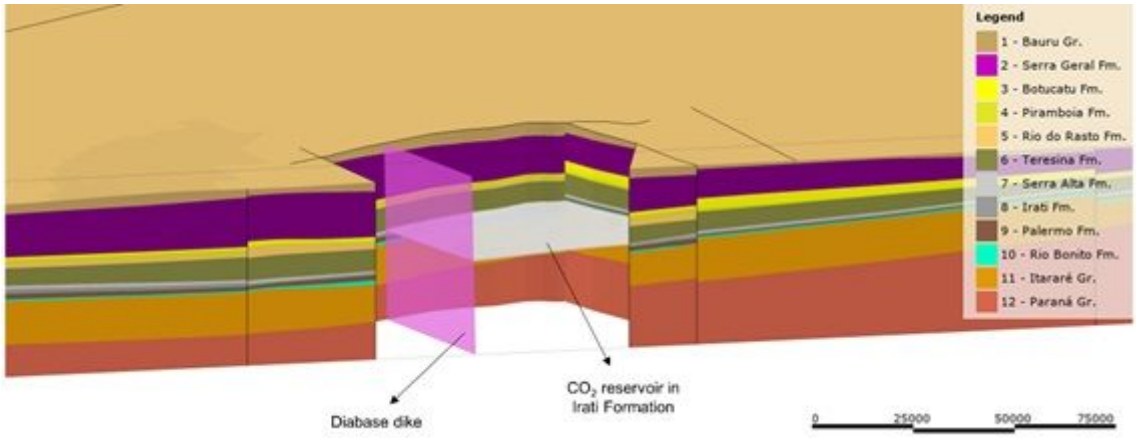

Figure 11

3D view with an E-W slice of the site location for CO2 storage used for calculation of theoretical capacity. Vertical scale = 10x.

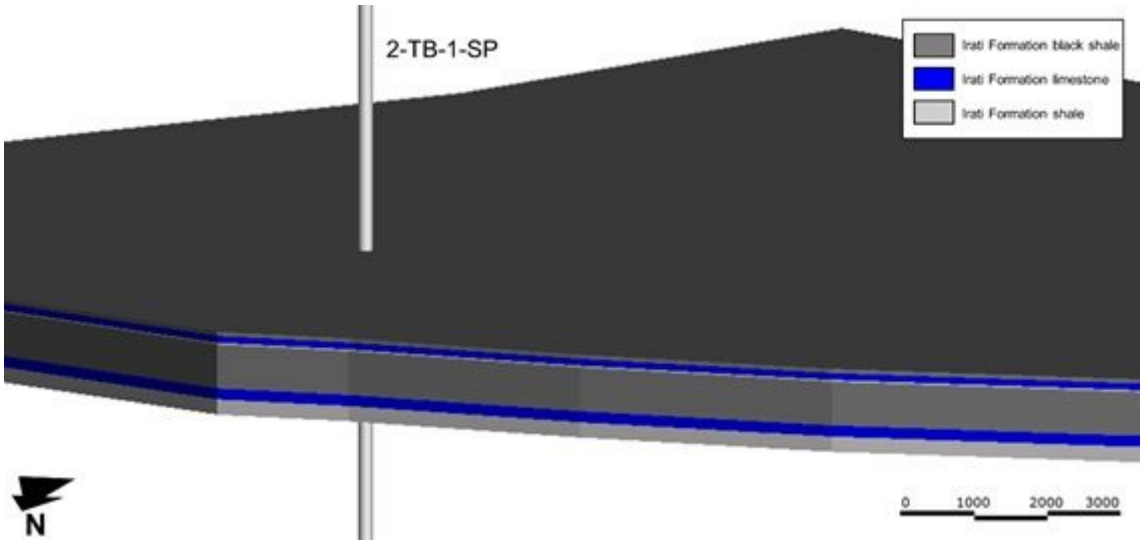

Figure 12

3D view of the local geological model of the CO2 reservoir with the well 2-TB-1-SP and geological units according to Fig. 3. Vertical scale = 30x.